Causes and consequences of asymmetric lateral plume flow during South Atlantic rifting

Jason P. Morgan[a,1], Jorge M. Taramón[b], Mario Araujo[c,d], Jörg Hasenclever[e], and Marta Perez-Gussinye[d]

[a]Department of Ocean Science and Engineering, Southern University of Science and Technology, 518055 Shenzhen, China; [b]Earth Sciences Department, Royal Holloway, University of London, TW2 0EX Egham, United Kingdom; [c]CENPES, Petrobrás, 21941-915 Rio de Janeiro, Brazil; [d]Center for Marine Environmental Sciences, University of Bremen, 330440 Bremen, Germany; and [e]Institute of Geophysics, Center for Earth System Research, Hamburg University, 20148 Hamburg, Germany

Edited by Donald W. Forsyth, Brown University, Providence, RI, and approved September 10, 2020 (received for review June 13, 2020)

Volcanic rifted margins are typically associated with a thick magmatic layer of seaward dipping reflectors and anomalous regional uplift. This is conventionally interpreted as due to melting of an arriving mantle plume head at the onset of rifting. However, seaward dipping reflectors and uplift are sometimes asymmetrically distributed with respect to the subsequent plume track. Here we investigate if these asymmetries are induced by preexisting lateral variations in the thickness of continental lithosphere and/or lithospheric stretching rates, variations that promote lateral sublithospheric flow of plume material below only one arm of the extending rift. Using three-dimensional numerical experiments, we find that South Atlantic rifting is predicted to develop a strong southward asymmetry in its distribution of seaward dipping reflectors and associated anomalous relief with respect to the Tristan Plume that "drove" this volcanic rifted margin, and that the region where plume material drains into the rift should experience long-lived uplift during rifting—both as observed. We conclude that a mantle plume is still needed to source the anomalously hot sublithospheric material that generates a volcanic rifted margin, but lateral along-rift flow from this plume, not a broad starting plume head, is what controls when and where a volcanic rifted margin will form.

mantle plumes | rifting | volcanic rifted margins

At a volcanic rifted margin, the transition from rifting to spreading is associated with the generation of much thicker than normal oceanic crust (1, 2), and the formation of pervasive magmatic seaward dipping reflectors (SDRs) (1, 3). Conventionally, this is interpreted as the byproduct of melting of hotter-than-average mantle associated with the recent arrival of a plume head in the region, the plume head's center being located near the starting point of the postrift "hotspot track" of seamount volcanism caused by melting in the upwelling plume conduit (4–6).

In the North Atlantic this spatial pattern crudely holds (Fig. 1*A*), with the Iceland hotspot track located roughly in the center of the region of SDRs associated with Greenland-European rifting. In contrast, South Atlantic rift-related volcanism does not fit this pattern, because the Tristan hotspot track is located near the northern edge of the region with SDRs (7) (Fig. 1*B*). Such an asymmetric relationship is not unique to the South Atlantic. For example, Seychelles/Deccan rifting over the Reunion plume has excess rifting-related volcanism along the Seychelles platform that lies to one side of the Chagos-Laccadive hotspot track of the Reunion Plume (8, 9).

Furthermore, the South Atlantic Margin also has a clearly anomalous pattern of subsidence before the time of SDR emplacement (Fig. 2 *A*–*C*) (10–12). The Santos and Campos basins near the latitude of the later Tristan Plume track experienced rifting without normal rift-related subsidence (11, 13, 14) (Fig. 2 *D*–*G*), which led to the development of a long-lived extended shallow carbonate platform (Fig. 2 *D*–*G*) and the formation of salt deposits in these basins (Fig. 2 *A*–*C*). Well-accepted reconstructions by Torsvik et al. (10) and Karner and Gamboa (11) imply this anomalous uplift occurred >10 My after the eruption of the Parana-Etendeka flood basalts, inconsistent with the interpretation of the conventional model that the generation of SDRs should reflect the time that the starting plume head first impacted the about-to-rift lithosphere.

Here we investigate a different plume-linked hypothesis for the generation of excess volcanism and SDRs during early plume-influenced continental rifting. In this scenario, lateral plume drainage is shaped by both lateral variations in the initial thickness of continental lithosphere, and along-strike variations in the geometry and opening rate along the rift. Numerical calculations predict that these tectonic variations will induce ponded plume material to be pulled southward from the Tristan plume during early South Atlantic rifting (see Fig. 3 *A*–*D* and *SI Appendix*, Animations 1–8).

Methods

This scenario, while simple in concept, is challenging to explore numerically as it involves both buoyant three-dimensional (3D) mantle flow and strong lateral variations in lithospheric strength/temperature that shape viscous mantle flow. To properly account for narrow plume conduits and the buoyancy effects of hot plume material requires high spatial resolution of order ~10 km or better. Usually this type of flow calculation has been done within a high-resolution regional model. The conundrum associated with this choice is that it requires the accurate definition of artificial boundary conditions around the region of interest that are difficult to apply in such a

Significance

This article tackles the longstanding question of why some continental rifting was associated with major pulses of excess volcanism that formed "volcanic rifted margins," yet other rifting, even nearby, was not. After reviewing the South Atlantic rifting exemplar, we present results from an improved type of three-dimensional calculation of mantle flow that avoids many of the artificial boundary condition-related pitfalls in prior numerical studies that did not predict asymmetric rift-related volcanism. Our experiments match the observed development of asymmetric volcanism during South Atlantic rifting, with important implications for plume-influenced rifting of continents. In particular, the scenario does not require a conventionally assumed "starting plume head" to provide the hotter-than-average mantle that induces excess rift magmatism.

Author contributions: J.P.M. and J.M.T. designed research; J.P.M., J.M.T., M.A., and J.H. performed research; J.P.M., J.M.T., M.A., J.H., and M.P.-G. analyzed data; and J.P.M., J.M.T., M.A., J.H., and M.P.-G. wrote the paper.

The authors declare no competing interest.

This article is a PNAS Direct Submission.

[1]To whom correspondence may be addressed. Email: jason@sustech.edu.cn.

This article contains supporting information online at https://www.pnas.org/lookup/suppl/doi:10.1073/pnas.2012246117/-/DCSupplemental.

First published October 26, 2020.

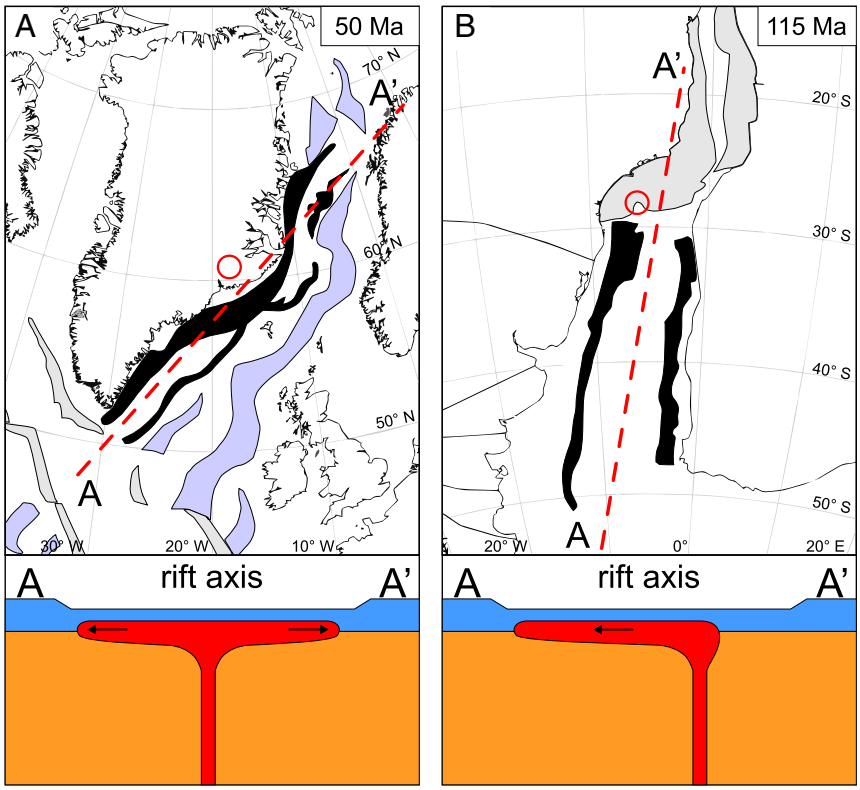

Fig. 1. Cartoon sketch of symmetric "North Atlantic" (*A*) and asymmetric "South Atlantic" (*B*) modes of plume–rift interaction. (*A*, *Top*) GPlates-based [Caltech_Global_20101129 (20)] reconstruction of the North Atlantic rift system at ~50 Ma. Black shows the extent of volcanic rifted margin/SDR rocks. Red circle shows inferred plume location at the time of formation of SDRs. Purplish areas show regions of earlier rift extension. (*A*–*A*′) Location of the cross-section shown at the bottom. (*Bottom*) Cartoon sketch of the proposed mode of lateral plume flow in a rift system with symmetric along-rift flow away from a centrally located plume source. This mode will happen if there are not strong lateral along-rift variations in age/thickness of the rifting lithosphere, and relatively uniform extension rates to the north and south of the plume source. (*B*, *Top*) GPlates-based [Caltech_Global_20101129 (20)] reconstruction of the South Atlantic rift system at ~115 Ma. Black and gray colors show the regional distribution of SDRs (volcanic rifted margin), and salt (nonvolcanic rifted margin). (*SI Appendix* contains further details.) Red circle shows inferred plume location around the time of formation of SDRs. (*Bottom*) Cartoon sketch of the proposed mode of asymmetric lateral flow along the rift system from a plume source that can lead to a South Atlantic-like distribution of volcanic and nonvolcanic rifted margins with respect to the plume source.

way that they do not artificially influence large-scale flow within the solution region. For example, a study by Burov and Gerya (15) to study the interaction of lithospheric stretching and a starting plume head used idealized boundary conditions that were a combination of pure and simple shear along the sidewalls of their computational box, free slip on any sidewalls without prescribed pure or simple shear, and material being allowed to flow into the top or base of the box to ensure mass conservation. A later 3D rifting study (16) used the same code to investigate plume–rift interaction beneath a segmented Iceland–Greenland-like rifting margin. For simplicity, the sidewalls in this 2,600 × 3,000-km-wide by 635-km-deep model region were treated as closed free-slip boundaries, a choice which led to the formation of artificial downwellings along the two sidewalls that opposed the rift axis. A "nested model" approach (compare refs. 17,18) was used to model the long-term interaction of the Tristan Plume with the evolving southern Mid-Atlantic Ridge (19). Here, boundary conditions for the computational region were determined from a coarser global solution that did not contain the same local plume fluxes. This choice has the potential advantage that it allows one to explore the far-field influence of global buoyancy-driven flow on the regional calculation (compare refs. 18,19) but it can be problematic if the global solution used to create the time-dependent regional boundary conditions does not accurately model the appropriate local plume inflow and its associated outflow from the region. Assumptions about where and how much outflow will occur to compensate for additional local plume inflow can also artificially influence the solution. For example, solutions in ref. 19 had relatively minor along-rift flow of plume material because their plume outflow was prescribed to occur in the plate-spreading direction.

Here we use a variable resolution global mesh (*SI Appendix*, Figs. S1 and S2) to circumvent these difficulties. A high-resolution (~10-km node spacing) portion of the mesh is generated within a subregion of interest (*SI Appendix*, Fig. S1*E*) that forms only a small volume fraction of a variable resolution global mesh designed to adequately resolve exterior large-scale mantle flow (*SI Appendix*, Figs. S1*A* and S2). In our models, ~70% of the mesh's degrees-of-freedom is concentrated within the high-resolution region of interest that contains only 0.25% of the total mantle volume. Buoyancy effects are only present within the high-resolution subregion. This approach avoids the need to accurately define artificial time-dependent side-boundary conditions around the high-resolution region of interest. The only boundary conditions needed in this approach are the standard assumption of free slip along the core–mantle boundary, and a prescribed evolution of global plate motions along Earth's surface. For consistency with previous studies, we use a well-accepted GPlates global plate motion history (Caltech_Global_20101129.rot and Caltech_Global_20101129.gpml) (20) (*SI Appendix*, Fig. S3) for the time interval of interest. Local plume inflow and temperature are imposed through use of a high-resolution cylindrical plume subregion that stretches from the base of the high-resolution portion of the mesh to 670-km depth. Within the 200-km-diameter plume cylinder, the plume's radial velocity distribution and excess temperature are prescribed to be a time-independent parabolic vertical upflow and a time-independent Gaussian temperature profile with a maximum temperature of 1,450 °C along the central axis of the plume that decreases to the background mantle temperature of 1300 °C along the outer radius of the plume. Temperature along the model's top surface is prescribed to be 0 °C, and along the core–mantle boundary surface is prescribed to be 1300 °C. (See *SI Appendix* for further details.). As buoyancy effects are only present within the high-resolution subregion, regional plume outflow will take the path of least resistance consistent with the regional viscosity structure and surface plate motions. The only bottleneck to this approach is the need to build an

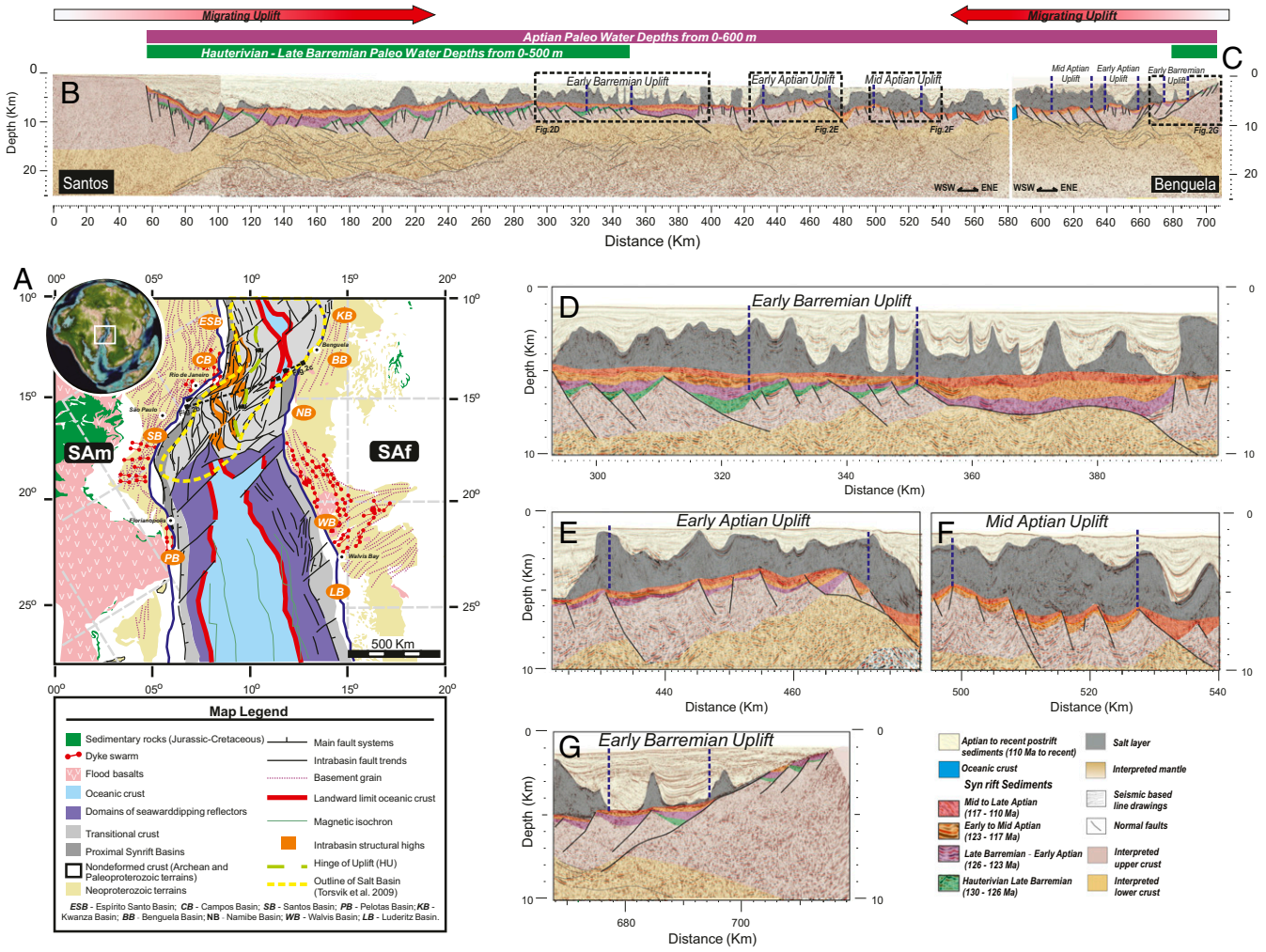

Fig. 2. (*A*) Africa (SAf) and South America (SAM) shown in a South Atlantic plate reconstruction for 117 Ma (12), with SAf fixed in present-day coordinates. Note the contrast of intrabasin architecture from north to south, with northern compartments defined by sigmoidal intrabasin fault trends that separate structural lows from structural highs. This region coincides with the area occupied by the Aptian Salt basins of Central Atlantic. Southward around ∼17°S, a succession of intrabasin highs and lows terminates abruptly against SDRs. This coincides with the boundary of the region with evidence of long-lived plume influence during rifting. The legend defines map symbols used. Modified from ref. 12, which is licensed under CC BY 3.0. Additional data from ref. 10. (*B* and *C*) Depth-converted conjugate Santos-Benguela transect through the central portion of Central Atlantic. This transect shows the surface at ∼117 Ma, but includes later deformation that is also present in the present-day seismic records. Transect location shown in Fig. 2*A*. Note that this margin is extremely asymmetric. (*B*) The wide margin, located in the Brazilian side, shows landward dipping normal faults, which change polarity to basinward faults after passing by a proximal dome defined by deep reflector bands buried below Late Barremian [126-123 Ma, deposited in shallow euxinic fresh water and alkaline lakes rich in magnesium (11, 13)] and Early Aptian [123–117 Ma, highly saline, deposited in arid shallow-water conditions (11, 14)] sediments. We interpret this feature to be exhumed lower crust. To its east, the upper crustal structure is defined by eastward-verging rotated blocks, with synrift sediments progressively younging oceanward, separated by basement hinges. (*C*) In its opposing conjugate side, the Benguela basin is extremely narrow, but shows a similar arrangement of ocean younging internal compartments. (*D*–*G*) Details of the synrift sedimentary infill and basement hinges that mark different uplift episodes associated with oceanward migration of deformation. Both margins are covered by salt layers and post-Aptian to modern sediments.

appropriate variable resolution mesh. For this we use an algorithm (21) inspired by the DISTMESH approach to mesh generation (22).

Lateral plume drainage is also sensitive to initial thickness variations in the prerift lithosphere. For example, Steinberger et al. (23) show an example of this where variable lithospheric thickness in the Greenland region affects the long-term flow of Iceland plume material. Here we define initial South American/African craton regions to have an initial lithospheric thickness of 240 km. Noncratonic/mobile belt regions are presumed to have a thinner initial lithospheric thickness of 130 km (Fig. 3 *A*, *Right Inset* and *SI Appendix*, Fig. S4). Craton distributions are taken from de Wit et al. (24). The 3D parallel-computation solutions discussed here were computed on a 2012 Dell workstation with 48 cores and 256 Gb of shared memory, with a typical run taking ∼3 wk to complete. *SI Appendix* contains a description of the numerical techniques and code, mesh generation, and boundary conditions used in these calculations.

Results

Early Evolution. Fig. 3 and *SI Appendix*, Animation 1 show a typical example of the evolution of along-rift flow of plume material for a plume source near the paleo-latitude of the Tristan Plume. Because of the combined effect of thicker cratonic lithosphere to the north (Fig. 3 *A*–*C*, *Right* and Fig. 4*C*) and lateral suction toward the more rapidly stretching rift sections to the south (Fig. 4*A*), plume material is preferentially pulled toward the southern sections of the rift. Progressive infill of buoyant hot plume material beneath the southern sections of the rift leads to corresponding asymmetric uplift of the rift regions that overlie plume material (Fig. 3 *A*–*D*, *Bottom Left Insets*, Fig. 3*E*, and *SI Appendix*, Animation 2), even when the lithosphere in these regions is still too thick for the plume material to

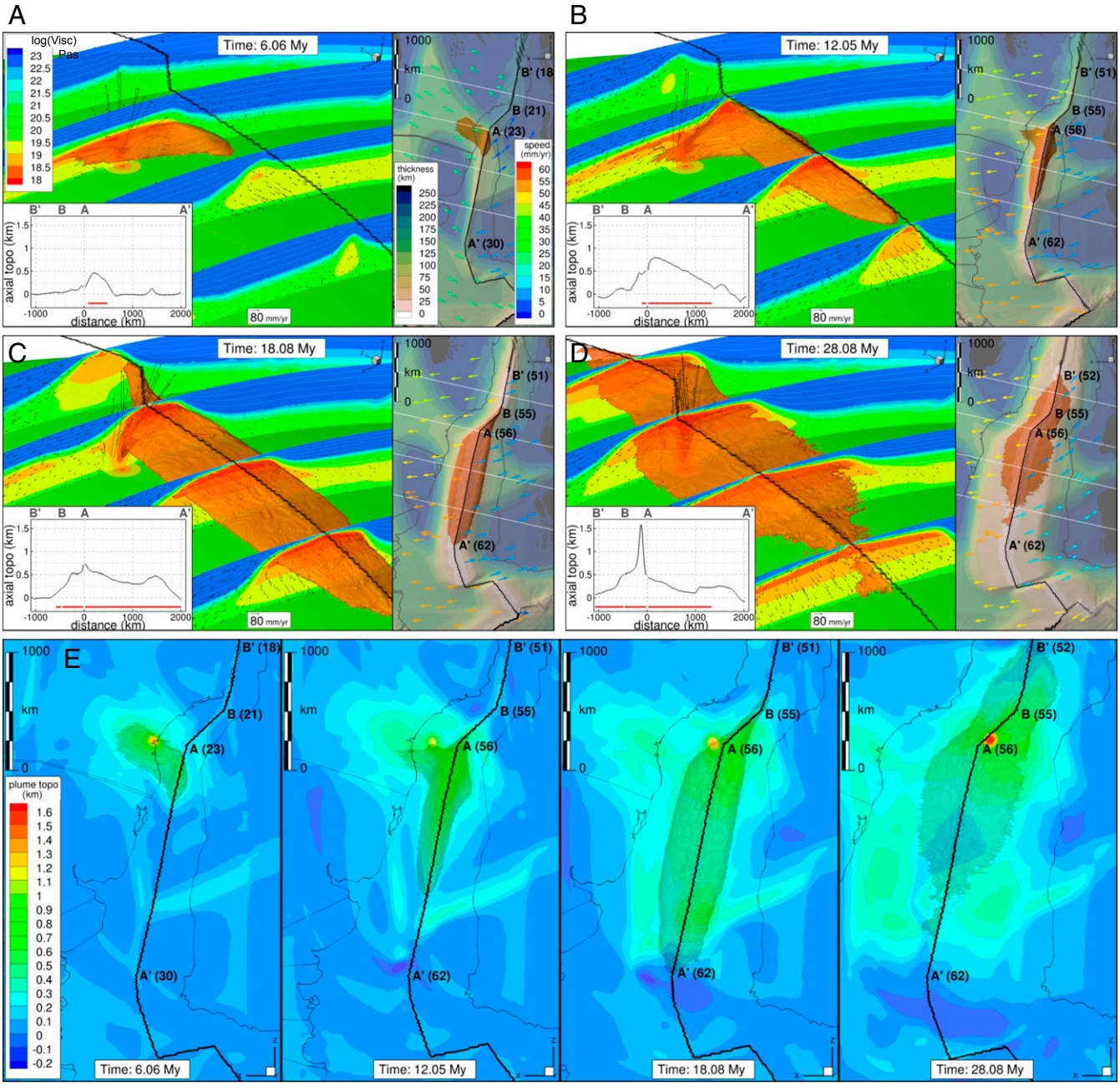

Fig. 3. (*A–D*) Snapshots of the 3D evolution of lateral plume transport beneath a South Atlantic scenario for plume–rift interaction for model L1F15 that assumes a plume flux of 15 km^3/y and the starting plume location shown in Fig. 4*B*. (*E*) Snapshots of the corresponding plume contribution to anomalous surface relief. Tecplot 360 was used to create these figure panels. (*A–D*) Three-dimensional images showing the geometry of the plume material at different times after rift initiation: (*A*) 6.06 My (e.g., ~124 Ma), (*B*) 12.05 My (~118 Ma), (*C*) 18.08 My (~112 Ma), and (*D*) 28.08 My (~102 Ma). Each primary panel shows a perspective view of the semitransparent isosurface of plume material superimposed onto a horizontal cross-section of the logarithm of viscosity at the base of the high-resolution subregion and four vertical cross-sections along the ridge axis. Colors represent the logarithm of viscosity in Pa-s (see color bar in *A*). The plume material is defined here by the semitransparent red isosurface of log(*Visc*/Pa-s) = 18.2. The velocity field and isotherms every 200 °C in the vertical cross sections are represented by arrows and white lines, respectively. Velocity arrow length scale for a speed of 80 mm/y = km/My is shown near the bottom of each panel. Black line represents the plate boundary. *Right*, subpanels: top view of the 3D evolution shown in the corresponding main panel. The isosurface with a temperature of 1,170 °C is colored as a function of depth to show the lithospheric thickness variations (see color bar in right subpanel of *A*). Plume material is represented by the semitransparent red isosurface of log(*Visc*/Pa-s) = 18.2. Color arrows represent top surface plate motion directions and speeds (see rainbow-colored bar in right subpanel of *A*). Gray lines and black thick lines represent reconstructed coastlines (including potential plate-reconstruction faultlines within continents) and plate boundaries, respectively. Capital letters show the ends of the along-ridge profiles shown in bottom left inset of each left panel. Numbers between () brackets show the full opening speed in mm/y. (*Insets*, *Bottom Left*) Plume contribution to axial topography in kilometers. The red horizontal line represents where plume material is present beneath the ridge profile. (*E*) Color maps of plume contribution to anomalous topography in kilometers, at the same times as *A–D*. Underlying plume material is represented by the semitransparent shaded isosurface of log(*Visc*/Pa-s) = 18.2. Black thin and thick lines represent reconstructed coastlines and the plate boundaries, respectively. Capital letters show the ends of the along-ridge profiles shown in *A–D*. Numbers in parentheses show the local full opening speed in km/My.

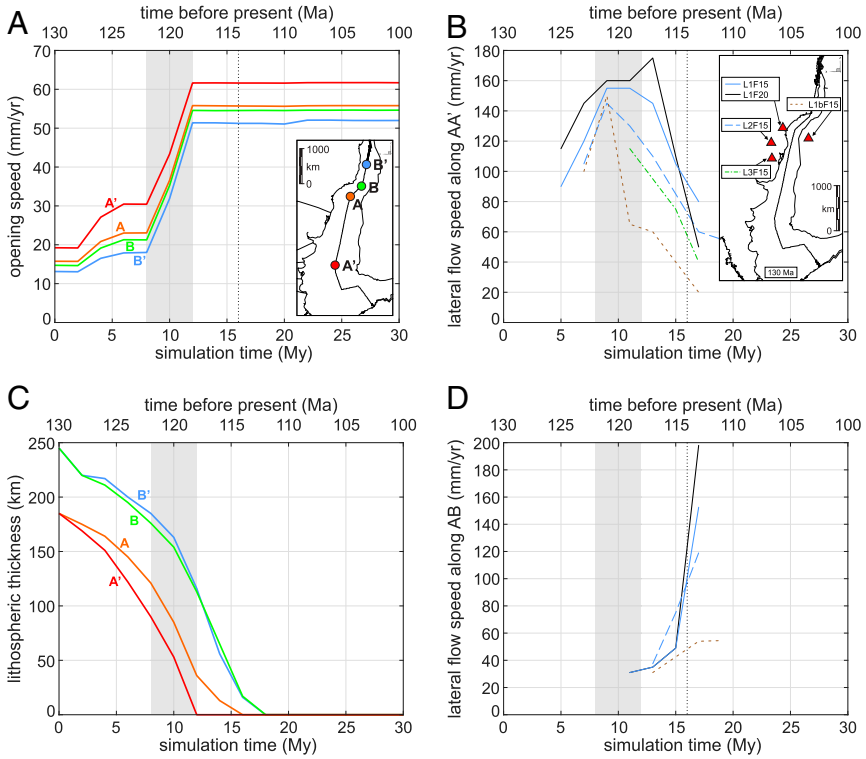

Fig. 4. (*A*) Full opening speed in mm/y of the South Atlantic between 130 and 100 Ma, taken from the Caltech_Global_20101129 (20) kinematic plate reconstruction. Capital letters refer to the ends of the profiles shown in the panel's inset. Gray color delimits the time with an abrupt acceleration in opening speed. (*B*) Average southward speed of plume material for every 2-My interval after the plume material reaches the rifting region. Speed is measured at the front of the migrating plume material. Vertical dotted line at 114 My marks the time when the northward passage between São Francisco and Congo cratons had opened enough to permit significant northward migration of plume material. Line colors and patterns are shown for model experiments with different plume fluxes (F15 =15 $km^3\ y^{-1}$, F20 = 20 $km^3\ y^{-1}$), and plume starting locations are shown by the red triangles in the inset to this panel. (*C*) Rift axis lithospheric thickness—defined at the depth of the 1,170 °C isotherm—as a function of time at locations A′, A, B, and B′. Note how the northern rift axis lithosphere is much thicker than rift lithosphere to the south, and only thins to <80 km at ∼117 Ma, ∼13 Ma after the onset of model rifting. Rifting lithosphere progressively thins southward because rift opening rates increase southwards (*A*). Lateral spatial variations in lithospheric thickness are also shown in snapshots in right-hand panels in Fig. 3*A*. (*D*) Average northward speed of plume material for every 2-My interval in the time interval when plume material began to rapidly move northward into the thinning rift system. Rapid northward flow starts ∼115 Ma, ∼15 Ma after the onset of model rifting. Line colors and patterns defined in *B*, *Inset*.

decompress enough to melt. Southward lateral flow beneath the rift is associated with small amounts of decompression induced by stretching and lithospheric thinning. However, the largest decompression and deepest decompression melting of plume material would only occur when it flows upward within its deeper quasivertical conduit and beneath the upward sloping sublithospheric region between the plume stem and rift axis (see Fig. 3 and *SI Appendix*, Animations 1 and 2). Fig. 3 *A–D*, *Bottom Left Insets* and Fig. 3*E* show the corresponding evolution of anomalous relief above the rifting region (also see *SI Appendix*, Animations 2 and 4). After 12 My, isostatic uplift from the thermal buoyancy of sublithospheric plume material is predicted to cause up to 800 m of regional uplift in the northern rift regions near the plume source, with anomalous relief slowly decreasing toward southern regions of the rift axis, and rapidly decreasing toward northern regions where plume material initially does not flow (Fig. 3 *B*, *C*, and *E*). As the lithosphere progressively thins along the rift, further decompression melting of underlying plume-fed material starts when the lithosphere has thinned to less than the solidus depth of this material. This occurs in the exact southern region where SDRs are associated with South Atlantic opening (compare Fig. 3*C* with Figs. 1*B* and 2). The southern extent of SDRs along the rift can be used to constrain the upwelling plume flux. Models with a constant plume flux between 15–20 km^3/y (also see *SI Appendix*, Fig. S5) produce patterns consistent with the observed distribution of SDRs (Fig. 1*B*).

Later Evolution. After ∼15 Ma of slow rifting, the cratonic rifting lithosphere to the north has thinned enough for plume material to start to flow more symmetrically north and south from the on-ridge projection of the plume (Fig. 3 *C* and *D* and *SI Appendix*, Animations 1 and 2). Initial slow northward migration of plume material is associated with concentrated uplift along the rift axis (see Fig. 3 *A–D* and *E* along the rift section A-B). After ∼15 Ma of rifting, material starts to rapidly flow northward at speeds of order 200 km/My (Fig. 4*D*), leading to the lateral along-rift flow along the oblique rift section A-B that has a faster eastward component of motion than its overlying east–west plate motions. This region of predicted focused uplift is similar in shape and close in location to the observed "hinge" of uplift in the Santos and Campos Basins (marked as HU in Fig. 2*A*). This is also the region where ultra-deepwater oil fields have been found offshore Brazil, suggesting a possible plume link to the early development of these systems.

At this point the southern regions become starved of their underlying plume material which has flowed toward, decompressed, and been consumed by rift stretching, while proximal regions north and south of the plume are still being supplied by local along-rift flow.

Similar patterns of plume flow are predicted to occur if the plume was initially located at a similar paleo-latitude on the African side of the proto-rift axis at location L1b in Fig. 4*B* (*SI Appendix*, Animations 7–8). Only when the initial plume is located ~1,000 km to the south (L3 in Fig. 4*B*), in a location completely inconsistent with the postrift location of the Walvis Ridge plume track, would initial rifting be associated with symmetric north- and southward expansion of plume material along the southern section of the South Atlantic Rift (*SI Appendix*, Animations 9–10).

The predicted time progression of plume-rift influence is the following:

1) Southward lateral plume flow beneath thinning rift lithosphere leads to anomalous uplift in the rift sections south of the proto-Tristan plume.
2) Significant sublithospheric melting starts only after the period of lateral infill of plume material, as the lateral infill phase itself is associated with little direct decompression-induced melting. After the lithosphere has thinned enough so that the plume material's temperature at the base of the lithospheric exceeds its solidus, then further decompression induced by rift stretching will be associated with SDR creation in the stretching regions which overlie warm plume material. This implies that SDR formation should occur after the onset of anomalous uplift, and well after the formation of the initial Tristan-plume-linked melting event that created the Parana-Entendeka flood basalts.
3) As the rifting rate increases, the region of plume influence along the evolving rift shrinks (Fig. 3 *C* and *D*). After breakup it becomes more nearly centered on the region where the plume is closest to the spreading center (Fig. 3*D*; also see ref. 25). This reflects the fact that the initial phase of slow rift extension creates relatively little sublithospheric space to "consume" plume material by plate stretching, thereby favoring long-distance lateral migration of lower viscosity plume material along the growing rift axis.

Discussion

This scenario for plume–rift interaction beneath geologically reasonable lithosphere with thicker prerift cratonic and thinner prerift mobile belt regions explains several apparent enigmas associated with South Atlantic rifting: 1) It explains why the main regions of SDR development lie south of the proto-Tristan Plume location and the postrift Tristan Plume location at the Walvis Ridge–Africa junction; 2) It offers a quantitative prediction of up to ~800 m of anomalous uplift from only the thermal buoyancy of sublithospheric plume material and lithospheric heating beneath rift sections near the plume–rift junction, with even more anomalous uplift possible from incorporation of plume melts, and heating from melt passage through this lithosphere (see ref. 26 for an assessment of these effects).

In this scenario there is no need for a starting plume head to create SDRs along a volcanic rifted margin. Instead, the combination of a preexisting plume and rifting could form SDRs, as seems clear for the cases of the Iceland (27) and Reunion/Deccan plumes (28). This scenario is consistent with the observation that rifting along the southern South Atlantic margins appears to start with an early magma-poor rift stage, and evolves to a magma-rich breakup stage (29), an observation inconsistent with straightforward interpretations of a plume-head source for the creation of SDRs (e.g., ref. 5). It is also consistent with the observed time lag between the onset of well-developed seafloor spreading to the south of Santos and its onset at Brazilian–Angolan rift zones to the north of the Campos Basin (Fig. 2*A*). Finally, it can explain the delayed subsidence of the Campos/Santos Basins (Fig. 2) as being a byproduct of these basins having remained along the northern edge of plume-to-rift drainage for over 15 My (Fig. 3*E*).

Even so, this scenario keeps the key idea that hot plume-sourced mantle is a key ingredient to create SDRs during rifting, with the combination of this anomalously hot mantle and the lithospheric thinning during rifting both playing a key role in the generation of SDRs. Finally, SDRs need not be centered around the plume itself. Instead, SDRs will form above sections of the rift that overlie regions where hot plume material has preferentially migrated and ponded. Lateral drainage of plume-sourced mantle will be shaped by both initial lithospheric thickness variations (19, 23, 30, 31) and along-rift variations in opening rate that preferentially "pull" plume material toward one side of the plume. We find the pulling effect of along-rift variations in opening rate dominates over subtle large-scale along-rift variations in initial lithospheric thickness. Calculations with a subtle initial 10-km-vertical/1,000-km-horizontal tilt of the base of the lithosphere toward or away from the proto-Tristan plume location showed very similar patterns of resulting along-rift flow.

The lateral extent and size of the SDR region is directly linked to the amount of plume material that can be pulled into the growing rift, e.g., to the plume flux and the time it drains beneath thinning lithosphere prior to breakup. The implied plume flux is large, e.g., ~10–20 km^3/y for the Tristan Plume, so that ~15 upwelling plumes of this size could counterbalance the ~300 km^3/y of oceanic lithospheric mantle that is currently being subducted. References 31–33 discuss further global implications of this potential mode of asthenospheric flow.

Apart from the "suction" effect linked to lithospheric thinning during rifting, drainage of plume material will also be influenced by lateral variations in initial lithospheric thickness. *SI Appendix*, Animations 5 and 6 show the evolution of a run with the plume initially passing beneath the South American craton. Once plume material has reached the rift axis by lateral upward flow along the base of the tilting lithosphere, it then drains along axis in the same southwards pattern as shown in Fig. 3.

A further consequence is that, for the Iceland plume, a shift in lithospheric drainage from westward toward Baffin Island to eastward toward the East Greenland/European rifted margin would naturally happen as Greenland/Europe migrated westward over the plume (23, 27). This shift in drainage could induce the large-scale jump in North Atlantic rifting from Baffin Bay to the East Greenland margin, as well as the development of SDRs during early rifting of the conjugate East Greenland and Norway margins.

The models explored in this study were intentionally constructed to contain as many based-on-prior-literature ingredients as possible, and—apart from the range of assumed plume fluxes—have not been "tuned" to create a better fit to observed structural patterns along the rift. In particular, the GPlates reconstruction used results in the plume being west of the Walvis Ridge–African coast junction at the time of breakup. A slightly more northeasterly initial location of the plume may better fit uplift observations in the Campos and Santos Basins. A more complex rift history with rift propagation (34), in particular in the region around the Rio Grande Rise/Walvis Ridge section of the rift, could potentially also create a better fit between model predictions and observations. Note that new rift segments could naturally propagate toward the Tristan plume. If lithospheric thinning is greater beneath faster rifting regions to the south, once filled with sublithospheric plume material, they would have a larger anomalous regional axial elevation. This would generate regional gravity spreading forces (35, 36) that favor the northward propagation of spreading centers toward the Tristan plume, consistent with the observed time evolution of early seafloor spreading in the South Atlantic (34).

Despite many model simplifications, the modeled patterns of predicted plume–rift interaction clearly show the potential for along-rift migration of plume material to shape the genesis of volcanic rifted margins and the development of SDRs, and anomalous uplift along sections of these margins. In particular, we demonstrate that the evolution of South Atlantic Rifting may have been dramatically influenced by early southward along-rift migration of Tristan Plume material.

Data Availability. The M3TET_SPH MATLAB code and its supporting data have been deposited in GitHub (https://github.com/JorgeTaramon/M3TET_SPH). All study data are included in the article and *SI Appendix*.

ACKNOWLEDGMENTS. We thank the editors and reviewers for their helpful comments, and Han Xie for help with preparing the final figures. The COMPASS project supported J.M.T.'s PhD work that created the 3D spherical codetools and the numerical experiments discussed in this study.

1. Á. Horni *et al*., "Regional distribution of volcanism within the North Atlantic Igneous Province" in *The NE Atlantic Region: A Reappraisal of Crustal Structure, Tectonostratigraphy and Magmatic Evolution*, G. Péron-Pinvidic, Ed. *et al*. (Geological Society, Special Publications, London, 2017), Vol. 447, pp. 105–125.
2. D. Franke, Rifting, lithosphere breakup and volcanism: Comparison of magma-poor and volcanic rifted margins. *Mar. Pet. Geol.* **43**, 63–87 (2013).
3. K. Hinz, *A Hypothesis on Terrestrial Catastrophes; Wedges of Very Thick Oceanward Dipping Layers Beneath Passive Continental Margins*, (Geologisches Jahrbuch Reihe Geophysik, 1981), Vol. 22, pp. 3–28.
4. W. J. Morgan, "Hotspot tracks and the opening of the Atlantic and Indian oceans" in *The Sea*, C. Emiliani, Ed. (Wiley, New York, 1981), Vol. 7, pp. 443–487.
5. R. White, D. McKenzie, Magmatism at rift zones: The generation of volcanic continental margins and flood basalts. *J. Geophys. Res.* **94**, 7685–7729 (1989).
6. M. A. Richards, R. A. Duncan, V. E. Courtillot, Flood basalts and hot-spot tracks: Plume heads and tails. *Science* **246**, 103–107 (1989).
7. C. McDermott, L. Lonergan, J. S. Collier, K. G. McDermott, P. Bellingham, Characterization of seaward-dipping reflectors along the South American Atlantic margin and implications for continental breakup. *Tectonics* **37**, 3303–3327 (2018).
8. J. J. Armitage, J. S. Collier, T. A. Minshull, T. J. Henstock, Thin oceanic crust and flood basalts: India-Seychelles breakup. *Geochem. Geophys. Geosyst.* **12**, 25 pp., 10.1029/2010GC003316 (2011).
9. R. A. Duncan, The volcanic record of the reunion hotspot. *Proc. Ocean Drill. Program, Sci. Results* **115**, 3–10 (1990).
10. T. H. Torsvik, S. Rousse, C. Labails, M. A. Smethurst, A new scheme for the opening of the South Atlantic Ocean and the dissection of an Aptian salt basin. *Geophys. J. Int.* **177**, 1315–1333 (2009).
11. G. D. Karner, L. A. P. Gamboa, "Timing and origin of the South Atlantic pre-salt sag basins and their capping evaporites" in *Evaporites Through Space and Time*, B. C. Schreiber, S. Lugli, M. Babel, Eds. (Geological Society, Special Publications, London, 2007), Vol. 285, pp. 15–35.
12. C. Heine, J. Zoethout, R. D. Müller, Kinematics of the South Atlantic rift. *Solid Earth* **4**, 215–253 (2013).
13. J. L. Dias, J. Q. Oliveira, J. C. Vieira, Sedimentological and stratigraphic analysis of the Lagos Feia formation, rift phase of Campos basin, offshore Brazil. *Rev. Bras. Geocienc.* **18**, 252–260 (1988).
14. H. K. Chang, R. O. Kowsmann, A. M. F. Figueiredo, A. Bender, Tectonics and stratigraphy of the East Brazil Rift system: An overview. *Tectonophys.* **213**, 97–138 (1992).
15. E. Burov, T. Gerya, Asymmetric three-dimensional topography over mantle plumes. *Nature* **513**, 85–89 (2014).
16. A. Koptev, S. Cloetingh, E. Burov, T. François, T. Gerya, Long-distance impact of Iceland plume on Norway's rifted margin. *Sci. Rep.* **7**, 10408 (2017).
17. E. Tan, E. Choi, P. Thoutireddy, M. Gurnis, M. Aivazis, GeoFramework: Coupling multiple models of mantle convection within a computational framework. *Geochem. Geophys. Geosyst.* **7**, 10.1029/2005GC001155 (2006).
18. P. Mihalffy, B. Steinberger, H. Schmeling, The effect of large-scale mantle flow on the Iceland Hotspot Track. *Tectonophys.* **447**, 5–18 (2008).
19. R. Gassmöller, J. Dannberg, E. Bredow, B. Steinberger, T. H. Torsvik, Major influence of plume-ridge interaction, lithosphere thickness variations, and global mantle flow on hotspot volcanism—The example of Tristan. *Geochem. Geophys. Geosyst.* **17**, 1454–1479 (2016).
20. M. Gurnis *et al*., Plate tectonic reconstructions with continuously closing plates. *Comput. Geosci.* **38**, 35–42 (2012).
21. J. M. Taramón, J. P. Morgan, C. Shi, J. Hasenclever, Generation of unstructured meshes in 2-D, 3-D, and spherical geometries with embedded high-resolution sub-regions. *Comp. Geosci.* **133**, 10.1016/j.cageo2019.104324 (2019).
22. P.-O. Persson, G. Strang, A simple mesh generator in MATLAB. *SIAM Rev.* **46**, 329–345 (2004).
23. B. Steinberger, E. Bredow, S. Lebedev, A. Schaeffer, T. H. Torsvik, Widespread volcanism in the Greenland–North Atlantic region explained by the Iceland plume. *Nat. Geo.* **12**, 61–68 (2019).
24. M. J. de Wit, J. Stankiewicz, C. Reeves, Restoring pan-African-Brasiliano connections: More Gondwana control, less trans-Atlantic corruption. *Geol. Soc. Lond. Spec. Publ.* **294**, 399–412 (2008).
25. G. E. Vink, A hotspot model for Iceland and the Voring Plateau. *J. Geophys. Res.* **89**, 9949–9959 (1984).
26. J. P. Morgan, W. J. Morgan, E. Price, Hotspot melting generates both hotspot volcanism and a hotspot swell? *J. Geophys. Res.* **100**, 8045–8062 (1995).
27. L. A. Lawver, R. D. Müller, Iceland hotspot track. *Geology* **22**, 311–314 (1994).
28. A. R. Basu, P. R. Renne, D. K. Dasgupta, F. Teichmann, R. J. Poreda, Early and late alkali igneous pulses and a high- 3 He plume origin for the Deccan Flood basalts. *Science* **261**, 902–906 (1993).
29. K. Becker *et al*., Asymmetry of high-velocity lower crust on the South Atlantic rifted margins and implications for the interplay of magmatism and tectonics in continental breakup. *Solid Earth* **5**, 1011–1026 (2014).
30. N. Sleep, Lateral flow and ponding of starting plume material. *J. Geophys. Res.* **102**, 10001–10012 (1997).
31. M. Yamamoto, J. P. Morgan, W. J. Morgan, "Global plume-fed asthenosphere flow: (1) Motivation and model development" in *Plumes, Plates, and Planetary Processes*, G. R. Foulger, D. M. Jurdy, Eds. (GSA Spec., Boulder, 2007), Vol. 430, pp. 189–208.
32. J. P. Morgan, J. Hasenclever, C. Shi, New observational and experimental evidence for a plume-fed asthenosphere. *Earth Planet. Sci. Lett.* **366**, 99–111 (2013).
33. J. P. Morgan, W. J. Morgan, Y.-S. Zhang, W. H. F. Smith, Observational hints for a plume-fed, suboceanic asthenosphere and its role in mantle convection. *J. Geophys. Res.* **100**, 12753–12767 (1995).
34. G. R. Vink, Continental rifting and the implication for plate tectonics reconstructions. *J. Geophys. Res.* **87**, 10677–10688 (1982).
35. J. P. Morgan, E. M. Parmentier, Causes and rate limiting mechanisms of ridge propagation: A fracture mechanics model. *J. Geophys. Res.* **90**, 8603–8612 (1985).
36. L. S. Mondy, P. F. Rey, G. Duclaux, L. Moresi, The role of asthenospheric flow during rift propagation and breakup. *Geology* **46**, 103–106 (2018).